Controlled synthesis of highly dispersed platinum nanoparticles in ordered mesoporous carbons†

Shou-Heng Liu,[a] Rong-Feng Lu,[b] Shing-Jong Huang,[a] An-Ya Lo,[a] Shu-Hua Chien[bc] and Shang-Bin Liu*[a]

Received (in Cambridge, UK) 26th May 2006, Accepted 19th June 2006
First published as an Advance Article on the web 6th July 2006
DOI: 10.1039/b607449a

A novel route has been developed to fabricate ordered carbon mesoporous materials with well-dispersed, highly stable Pt nanoparticles of *ca.* 2–3 nm on the pore walls using platinum acetylacetonate as the co-feeding carbon and Pt precursor.

Recent developments in the fabrication of porous carbon supports with high surface areas, controlled porosity, and hence a propensity towards lowering the metal catalyst loading have received considerable attention in the R&D of electrode catalysts for fuel cells.[1–9] Among them, precious-metal incorporated carbon mesoporous materials (CMMs)[10,11] have been extensively studied particularly for their applications as carriers for hydrogen storage[12] and as catalyst supports for fuel cells.[3–9] It is well-known that the properties of the incorporated metals depend strongly on their particle size, shape, and dispersion. Conventional techniques for embedding platinum or mixed-metal nanoparticles in the porous supports typically invoke post-synthesis treatment either by impregnation,[5–7,10f] adsorption,[2b] or ion-exchange[13] methods. However, these aforementioned methods normally lead to uncontrolled growth of metal particle size and shape and aggregation/sintering at elevated temperatures due to minimization of the surface chemical potential.

Here we report a novel procedure for synthesizing a new mesoporous platinum–carbon nanocomposite based on the pyrolysis of carbon and Pt precursors in a mesoporous silica, such as SBA-15.[14] However, unlike previous attempts by which Pt(0) clusters with an average diameter of 10–40 nm were found to be either buried in the glassy carbon matrix[15] or on the exterior surfaces of the carbon rod,[4,5] our samples prepared by direct replicated synthesis using organometallic compounds as the Pt precursor and co-feeding secondary carbon source result in nanosized Pt(0) particles with an average diameter of *ca.* 2–3 nm studded on the interior pore walls of the tubular CMM. As will be discussed later, the Pt-CMMs so fabricated possess highly stable, well-dispersed Pt nanoparticles that are exposed to the environment and hence render applications not only as adsorbents for hydrogen storage but also as carbon monoxide-tolerant electrocatalytic materials for direct methanol (DMFC) and proton exchange membrane fuel cells (PEMFC).

[a]*Institute of Atomic and Molecular Sciences, Academia Sinica, Taipei 10617, Taiwan. E-mail: sbliu@sinica.edu.tw; Fax: +886-2-2362-0200; Tel: +886-2-2366-8230*
[b]*Institute of Chemistry, Academia Sinica, Taipei 11529, Taiwan*
[c]*Dept. of Chemistry, National Taiwan University, Taipei 10617, Taiwan*
† Electronic supplementary information (ESI) available: Characterization methods, Pt dispersion measurements, CO tolerance tests and evaluation of electrocatalytic performances. See DOI: 10.1039/b607449a

The SBA-15 mesoporous silica template was synthesized according to the procedures reported earlier.[14] Further direct replication of SBA-15 material into Pt-CMMs were carried out by the following steps: (i) about 0.5 g of calcined SBA-15 was dehydrated at 673 K for 4 h under vacuum; (ii) varied amounts of platinum acetylacetonate (Pt(acac); 98%, Acros) were dispersed in the furfuryl alcohol (FA; 98%, Acros) and trimethylbenzene (TMB; 98%, Acros) under ultrasonication; (iii) oxalic acid (98%, Acros) was used as the acid catalyst for polymerization of the FA solution; (iv) the mixture solution infiltrated in SBA-15 by incipient wetness impregnation at room temperature, followed by polymerization at 333 K then at 353 K, each for 12 h in air; (v) the resultant composite was treated at 423 K for 3 h, ramped to 573 K with a heating rate of 1 K min^{-1}, then to 1073 K with a heating rate of 5 K min^{-1} and maintained at that temperature for 3 h; (vi) the carbonization procedure was performed under vacuum; (vii) finally, the resultant black powders were leached with HF (1 wt%) aqueous solution for at least 24 h to remove the silica template, washed with distilled water and alcohol, then dried at 373 K to obtain the Pt-CMMs. Samples were characterized by various analytical and spectroscopic techniques, as described in the ESI.†

As shown in Fig. 1a, the XRD pattern observed for CMM synthesized in the absence of organometallic $Pt(CH(COCH_3)_2)_2$

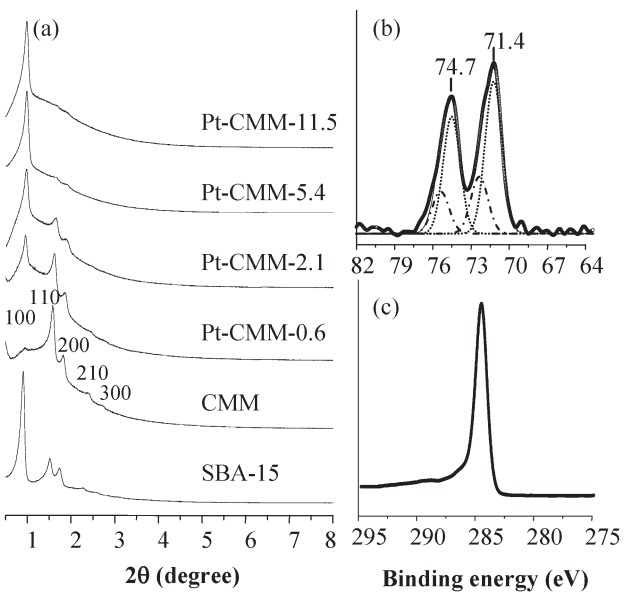

Fig. 1 (a) Powder XRD patterns of SBA-15, CMM, and various Pt-CMMs samples; (b) platinum XPS spectrum of Pt-CMM-0.6; (c) carbon XPS spectrum of Pt-CMM-0.6.

precursor exhibits well-resolved diffraction peaks, indicating the existence of long-range structural order with 2D hexagonal symmetry similar to that of the tubular CMK-5 material.[10f] Upon introducing the Pt precursor during synthesis, notable variations in the XRD patterns were found, revealing that the size and density of the Pt particles have substantial influence on the structure of the carbon support formed. This finding is in agreement with that concluded earlier by Xiao and co-workers[5] using an inorganic Pt precursor, namely $Pt(NH_3)_4(NO_3)_2$. As the Pt loading increased from 0.6 to 11.5 wt%, the XRD patterns progressively shift toward a closer resemblance of CMK-3,[10c–e] which represents a rod-like graphitized carbon replica of SBA-15. Large-angle XRD patterns observed for Pt-CMMs showed pronounced peaks at $2\theta = 39.8^\circ$, 46.2°, 67.8°, and 81.3°, especially for high Pt loading samples,† in accordance with those of crystalline platinum metal Pt(0) with a face centered cubic (fcc) lattice. Based on the Scherrer formula,† the average size of Pt deduced from the XRD profiles of the Pt-CMM-5.4 and Pt-CMM-11.5 samples were found to be 2.4 and 2.8 nm, respectively, coinciding with those determined from TEM images (see below).

X-Ray photoelectron spectroscopy (XPS) was also used to characterize the nature of platinum and carbon species, as exemplified by the results obtained from the Pt-CMM-0.6 sample in Fig. 1b and 1c. The Pt XPS spectrum in Fig. 1b could be deconvoluted into two pairs of doublets with intense peaks centered at binding energies of 71.4 and 74.7 eV, respectively. These two peaks are attributed to Pt $4f_{7/2}$ and Pt $4f_{5/2}$ excitations of metallic platinum, whereas the other weaker peaks at 72.2 and 75.5 eV are due to oxidized platinum. Thus, it is indicative that a substantial amount of Pt(acac) was reduced to metallic Pt(0) during pyrolysis of FA. On the other hand, the C 1s XPS spectrum of the Pt-CMM-0.6 sample in Fig. 1c consists of a sharp peak at *ca.* 284.5 eV, which could be attributed to the sp^2 graphitic carbon species. That this peak has a full-width at half-maximum (FWHM) linewidth of 0.9 eV, close to that of graphitized carbon black (0.82 eV),[16] revealing a well-ordered packing of graphene layers. Additional XPS experiments showed no detectable traces of Si and F in CMM and Pt-CMMs samples.

All N_2 sorption isotherms obtained from SBA-15, CMM, and Pt-CMM samples showed typical type-IV isotherms with well-defined hysteresis loops.† Accordingly, their structural parameters are summarized Table 1. All CMM and Pt-CMMs samples were found to possess high BET surface areas compared to their SBA-15 template. In particular, the BJH pore sizes obtained from the adsorption curves of CMM and Pt-CMM-0.6 samples revealed the existence of bimodal pore distributions. For the CMM sample, the larger pore with a diameter of 4.4 nm may be ascribed to the tubular carbon, whereas the smaller pore (2.3 nm) arises from the space interconnecting the carbon tubules formed after removal of the silica template. The wall thickness of the tubular CMM was found to be *ca.* 2–3 nm, as estimated from its TEM image and unit cell parameter. Moreover, all Pt-CMMs were found to possess micropores (pore size *ca.* 0.5–0.6 nm) in the carbon pore walls.†

All TEM images of the CMM and Pt-CMMs samples exhibited a uniform array of mesopores with long-range order, as illustrated in Fig. 2 for the Pt-CMM-0.6 sample. Pt metal particles with an average particle size of *ca.* 2–3 nm are uniformly dispersed throughout the sample (Fig. 2a) even at high loading.† A blown-up TEM image in Fig. 2b shows the existence of circular pores

Table 1 Physical properties of SBA-15, CMM and Pt-CMMs obtained from N_2 adsorption–desorption measurements at 77 K

Sample	Pt (wt%)	a^a/nm	S^b/m^2 g^{-1}	d^c/nm	V^d/cm^3 g^{-1}	D^e (%)
SBA-15	—	11.6	940	10.0	1.45	—
CMM	—	10.9	2 195	2.3; 4.4	1.67	—
Pt-CMM-0.6	0.6	10.6	1 818	2.3; 4.0	1.30	65
Pt-CMM-2.1	2.1	10.5	1 591	2.3	1.09	47
Pt-CMM-5.4	5.4	10.5	1 362	2.3	0.91	35
Pt-CMM-11.5	11.5	10.3	997	2.3	0.65	29
Pt-CMM-0.6I[f]	0.6	10.9	1 508	2.4; 4.3	1.16	16

[a] Unit cell parameter. [b] BET surface area. [c] BJH pore diameter. [d] Total pore volume. [e] Pt dispersion measured by H_2 chemisorption at 305 K. [f] Sample prepared by conventional impregnation method.

with size of 2.3 nm (brighter stripes) and tubular carbon studded with Pt particles (darker stripes), whereas the insert shows the image along the [100] direction. By comparison, the sample prepared by using the conventional post-synthesis impregnation method led to formation of a much wider distribution of Pt particle size, typically in the range of *ca.* 20 nm† (which is much greater than that of the dual pore sizes listed in Table 1) observed for Pt-CMM-0.6I. As such, the majority of the Pt particles should be present on the external surfaces of sample particulates rather than in the pore channels of carbon tubules.

Upon increasing Pt loading, gradual decreases in unit cell parameter (*a*), surface area (*S*), and pore volume (*V*) were observed for Pt-CMMs, indicating a gradual increase in the carbon wall thickness. This observation is in accordance with the diminishment of the pore with the larger diameter (while the smaller pore with pore size of 2.3 nm remains practically intact)† and the variations in the XRD profile (Fig. 1a) observed for Pt-CMMs with Pt loading exceeding 0.6 wt% (Table 1).

Thus, the overall synthesis scheme for the Pt-CMMs may be summarized based on the above findings, as illustrated in Fig. 3. This novel procedure is based on the pyrolysis of FA and $Pt(CH(COCH_3)_2)_2$ as carbon precursors in mesoporous silica SBA-15 template (Fig. 3a). In this case, the organometallic Pt(acac) not only serves as the Pt source but also as the secondary carbon source.[17] The substrate infiltrated with Pt and carbon precursors was then subjected to carbonisation at 1073 K under vacuum (Fig. 3c), followed by removal of the silica template with hydrofluoric acid solution, washing, and drying to obtained the final Pt-CMM product (Fig. 3d and 3e). Unlike the more conventional replication procedure for the synthesis of tubular

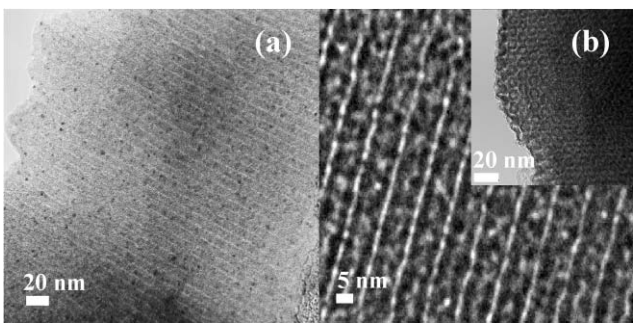

Fig. 2 (a) and (b) TEM images of tubular Pt-CMM-0.6 sample. Insert: image along the [100] direction.

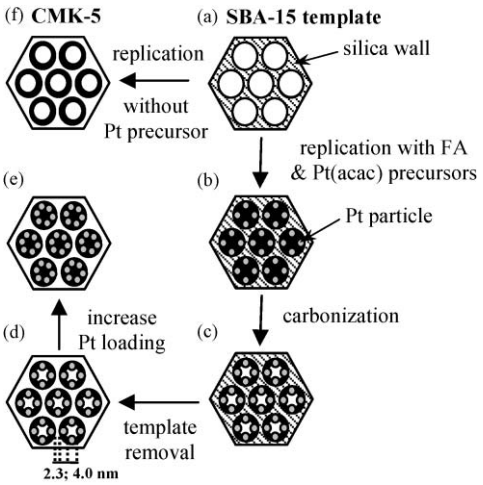

Fig. 3 Schematic drawings of synthesis routes for (a) → (e) Pt-CMMs, and (a) → (f) CMK-5.

mesoporous carbon CMK-5, which may be achieved in the absence of a Pt precursor (route from Fig. 3a to 3f),[10f] the synthetic route (from Fig. 3a through 3d) reported here results in uniform formation of Pt nanoparticles 2–3 nm in size in the inner pore walls of the tubular carbons. Consequently, two types of pores with respective diameters of 2.3 and 4.0 nm were identified especially for samples with low Pt loading, *e.g.*, Pt-CMM-0.6. Upon increasing the Pt loading (>0.6 wt%), Pt-CMMs with structures resembling that of rod-like CMK-3[10c–e] (Fig. 1a) but studded with well-dispersed Pt nanoparticles (Fig. 3e) were generated. As such, only one type of mesopore with a diameter of 2.3 nm was found. It is noted that the Pt metal particles in these Pt-CMMs are highly stable and sustain repeated oxidation and reduction cycles.

The dispersions of Pt nanoparticles in various samples obtained from H_2 chemisorption studies† are also depicted in Table 1. The Pt dispersion observed for the Pt-CMM-0.6 sample was found to increase by about four-fold compared to that of the Pt-CMM-0.6I prepared by the conventional impregnation method. For Pt-CMMs, a gradual decrease in Pt dispersion with increasing Pt loading was observed, as expected. Separate hydrogen uptake experiments performed under 113.3 kPa at 77 K showed that the H_2 adsorption capacity for Pt-CMM-0.6 amounts to 2.06 wt% corresponding to an increase of *ca.* 25% compared to that of Pt-CMM-0.6I (not shown). To investigate the CO tolerance of Pt-CMMs, we conducted additional pulsed chemisorption studies by competitive adsorption of CO with H_2.† Accordingly, a metallic surface area of *ca.* 190 m^2 $g(Pt)^{-1}$ for the Pt-CMM-0.6 sample was deduced in which *ca.* 78% remained active after pre-adsorption of 500 ppm of CO. In the case of Pt-CMM-0.6I, however, nearly all Pt surfaces were inactivated after exposure to the pre-adsorbed CO.

To evaluate the electrocatalytic activity of Pt-CMMs during methanol oxidation reaction, we also performed cyclic voltammetry (CV) in sulfuric acid.† Specifically, we compared the performances of our Pt-CMM-11.5 sample with a commercial Pt/C catalyst (Johnson-Matthey; 20 wt% Pt on Vulcan XC-72). It was found that our sample exhibits a catalytic activity surpassing that of the commercial catalyst. In particular, a lower oxidation peak potential was observed for the Pt-CMMs. In terms of the ratio of the forward anodic peak current density (I_f) to the reverse anodic peak current density (I_b), the I_f/I_b value obtained for the Pt-CMM-11.5 was 4.23, which amounts to about a four-fold increase compared to that of the commercial Pt/C catalyst, indicating that the latter is more vulnerable to coking by carbonaceous deposits[18] and less tolerant towards CO poisoning. Further studies are being undertaken to investigate the detailed mechanism of CO tolerance of Pt-CMMs and to fabricate various metal and bi-metal supported CMMs.

Notes and references

1 (*a*) A. Roucoux, J. Schulz and H. Patin, *Chem. Rev.*, 2002, **102**, 3757; (*b*) J. M. Thomas, B. F. Jhonson, R. Raja, G. Sankar and P. A. Midgley, *Acc. Chem. Res.*, 2003, **36**, 20; (*c*) K. Y. Chan, J. Ding, J. Ren, S. Cheng and K. Y. Tsang, *J. Mater. Chem.*, 2004, **14**, 505.
2 (*a*) G. Wang, G. Sun, Z. Zhou, J. Liu, Q. Wang, S. Wang, J. Guo, S. Yang, Q. Xin and B. Yi, *Electrochem. Solid-State Lett.*, 2005, **8**, A12; (*b*) R. Ubago-Pérez, F. Carrasco-Marín and C. Moreno-Castilla, *Appl. Catal., A*, 2004, **275**, 119.
3 (*a*) G. S. Chai, S. B. Yoon, J. S. Yu, J. H. Choi and Y. E. Sung, *J. Phys. Chem. B*, 2004, **108**, 7074; (*b*) G. S. Chai, S. B. Yoon, J. H. Kim and J. S. Yu, *Chem. Commun.*, 2004, 2766.
4 W. C. Choi, S. I. Woo, M. K. Jeon, J. M. Sohn, M. R. Kim and H. J. Jeon, *Adv. Mater.*, 2005, **17**, 446.
5 J. Ding, K. Y. Chan, J. Ren and F. S. Xiao, *Electrochim. Acta*, 2005, **50**, 3131.
6 F. Su, J. Zeng, X. Bao, Y. Yu, J. Y. Lee and X. S. Zhao, *Chem. Mater.*, 2005, **17**, 3960.
7 (*a*) V. Raghuveer and A. Manthiram, *Electrochem. Solid-State Lett.*, 2004, **7**, A336; (*b*) V. Raghuveer and A. Manthiram, *J. Electrochem. Soc.*, 2005, **152**, A1504.
8 K. Wlkander, H. Ekstrom, A. E. C. Palmqvist, A. Lundblad, K. Holmberg and G. Lindbergh, *Fuel Cells*, 2006, **6**, 21.
9 J. B. Joo, P. Kim, W. Kim, J. Kim and J. Yi, *Catal. Today*, 2006, **111**, 171.
10 (*a*) R. Ryoo, S. H. Joo and S. Jun, *J. Phys. Chem. B*, 1999, **103**, 7743; (*b*) M. Kaneda, T. Tsubakiyama, A. Carlsson, Y. Sakamoto, T. Ohsuna, O. Terasaki, S. H. Joo and R. Ryoo, *J. Phys. Chem. B*, 2002, **106**, 1256; (*c*) S. Jun, S. H. Joo, R. Ryoo, M. Kruk, M. Jaroniec, Z. Liu, T. Ohsuna and O. Terasaki, *J. Am. Chem. Soc.*, 2000, **122**, 10712; (*d*) S. H. Joo, R. Ryoo, M. Kruk and M. Jaroniec, *Chem. Commun.*, 2001, 349; (*e*) S. H. Joo, R. Ryoo, M. Kruk and M. Jaroniec, *J. Phys. Chem. B*, 2002, **106**, 4640; (*f*) S. H. Joo, S. J. Choi, I. Oh, J. Kwak, Z. Liu, O. Terasaki and R. Ryoo, *Nature*, 2001, **412**, 169.
11 (*a*) H. Darmstadt, C. Roy, S. Kaliaguine, S. J. Choi and R. Ryoo, *Carbon*, 2002, **40**, 2673; (*b*) H. Darmstadt, C. Roy, S. Kaliaguine, T.-W. Kim and R. Ryoo, *Chem. Mater.*, 2003, **15**, 3300; (*c*) B. Sakintuna and Y. Yürüm, *Ind. Eng. Chem. Res.*, 2005, **44**, 2893.
12 (*a*) J. Pang, J. E. Hampsey, Z. Wu, Q. Hu and Y. Lua, *Appl. Phys. Lett.*, 2004, **85**, 4887; (*b*) R. Gadiou, S.-E. Saadallah, T. Piquero, P. David, J. Parmentier and C. Vix-Guterl, *Microporous Mesoporous Mater.*, 2005, **79**, 121; (*c*) B. Z. Fang, H. S. Zhou and I. Honma, *J. Phys. Chem. B*, 2006, **110**, 4875.
13 V. Lordi, N. Yao and J. Wei, *Chem. Mater.*, 2001, **13**, 733.
14 D. Zhao, J. Feng, Q. Huo, N. Melosh, G. H. Fredrickson, B. F. Chmelka and G. D. Stucky, *Science*, 1998, **279**, 548.
15 (*a*) N. L. Pocard, D. C. Alsmeyer, R. L. McCreery, T. X. Neenan and M. R. Callstrom, *J. Am. Chem. Soc.*, 1992, **114**, 769; (*b*) H. D. Hutton, N. L. Pocard, D. C. Alsmeyer, O. J. A. Schueller, R. J. Spontak, M. E. Huston, W. Huang, R. L. McCreery, T. X. Neenan and M. R. Callstrom, *Chem. Mater.*, 1993, **5**, 1727.
16 (*a*) H. Darmstadt, C. Roy, S. Kaliaguine, S. J. Choi and R. Ryoo, *Carbon*, 2002, **40**, 2673; (*b*) H. Darmstadt, C. Roy, S. Kaliaguine, T.-W. Kim and R. Ryoo, *Chem. Mater.*, 2003, **15**, 3300; (*c*) B. Sakintuna and Y. Yürüm, *Ind. Eng. Chem. Res.*, 2005, **44**, 2893.
17 N. Toshima and K. Hirakawa, *Polym. J. (Tokyo)*, 1999, **31**, 1127.
18 J. Huang, Z. Liu, C. He and L. M. Gan, *J. Phys. Chem. B*, 2005, **109**, 16644.